Calculation of intensities in grazing-emission x-ray fluorescence

H. P. Urbach and P. K. de Bokx
Philips Research Laboratories, Professor Holstlaan 4, 5656 AA Eindhoven, The Netherlands
(Received 19 May 1995)

The sensitivity of x-ray fluorescence spectroscopy to surface and subsurface layers in the nanometer regime can be greatly enhanced by measuring the fluorescence radiation that is emitted at grazing angles. In this paper, we present a formalism for the calculation of x-ray fluorescence intensities that is also valid under grazing-emission conditions. By applying asymptotics to plane-wave expansions, an approximate solution to Maxwell's equations for a radiating point source in a layered system is derived, without the use of the optical reciprocity theorem. In the computation of the fluorescence intensity, secondary and higher-order fluorescence effects are taken into account. The total fluorescence of a particular layer is obtained by integrating the contributions of point sources at different depths. The derived expressions compare well with the measured angular dependence of the fluorescence intensity in a number of typical examples.

I. INTRODUCTION

The use of grazing-incident x-ray beams for the spectrochemical analysis of solid samples was first reported by Yoneda and Horiuchi.[1] Irradiating a sample at angles with the sample surface that are smaller than the critical angle for total reflection has the advantage that, at these angles, the x-ray penetration depth is extremely small. Contributions to the background spectrum from radiation scattered, by the bulk of the sample are considerably reduced and the sensitivity to surface constituents is greatly enhanced. The technique, commonly known as total-reflection x-ray fluorescence spectrometry (TXRF), has found wide application. Its main uses are the analysis of small amounts on top of an optically flat substrate[2,3] and the analysis of contaminants on semiconductor wafers.[4,5]

In the case of layered samples that have several distinct optical interfaces with associated critical angles, standing wave patterns may be generated inside the layered system, due to the interference of the incident beam and beams reflected from optical interfaces. From the angular dependence of the fluorescence intensity, one can infer the composition, the thickness, and the density of thin films and layers.[6,7] It has been stated that variable angle TXRF will become an established test method for layered samples in semiconductor technology and materials science.[8]

Becker, Golovchenko, and Patel[9] have demonstrated that the optical reciprocity theorem implies that x-ray fluorescence spectroscopy can be made surface sensitive not only by means of grazing-incidence, but also by means of grazing-emission techniques, i.e., by detecting only that part of the fluorescence radiation that is emitted at grazing angles. Grazing-emission XRF (GEXRF) has been applied to the analysis of ultrathin films on semiconductors[10] and to the analysis of ion implantation profiles.[11] Noma and Iida[12,13] have reported the interference of fluorescence x rays from thin film samples, using synchrotron radiation. Recently, we observed the same phenomenon using a laboratory instrument.[14] Compared with grazing-incidence methods, grazing-emission techniques have the advantage that they allow the use of wavelength-dispersive detection. Crystal monochromators have a much better wavelength resolution and sensitivity at long wavelengths than the solid-state detection devices used in TXRF.

In the theoretical description of grazing-emission fluorescence, the reciprocity theorem has been invariably used to calculate the fluorescence intensity, as a function of the emission angle. The theorem states that two sufficiently small dipoles radiating at the same frequency with moments $\mathbf{P}_1$ and $\mathbf{P}_2$ satisfy: $\mathbf{E}_1(2)\cdot\mathbf{P}_2=\mathbf{E}_2(1)\cdot\mathbf{P}_1$, where $\mathbf{E}_1(2)$ is the electric field induced by $\mathbf{P}_1$ at the position of $\mathbf{P}_2$ and $\mathbf{E}_2(1)$ is the electric field of $\mathbf{P}_2$ at $\mathbf{P}_1$.[15] This implies that the fluorescence intensity of a characteristic wavelength, emitted at grazing angles, can be calculated by interchanging the detector and the radiating atoms. Hence, the calculation is carried out as though we were dealing with an absorption experiment performed with radiation of the characteristic wavelength emitted by an imaginary source at the position of the detector. Because it is assumed that the wave incident on the sample due to this source is plane, the field inside the multilayer can be readily calculated using well-known recursion formulas.[16]

Although the reciprocity theorem is an elegant tool for deriving the fluorescence intensity at grazing angles, we will not apply it, but instead consider directly the field of a radiating source inside the sample. By asymptotic expansion of the integral over plane waves, occurring in the expression for the far field at the detector due to the radiating source, we obtain a closed formula for the fluorescence intensity of the radiating source, due to a single atom. The total fluorescence is then found by integrating over a distribution of atoms. In Secs. II and III, expressions will be derived for the fluorescence intensity from the upper and lower layers of a two-layer sample.

The motivation for this approach is twofold. First, the asymptotic analysis gives an indication of the range of emission angles for which the approximate expression for the fluorescence intensity is sufficiently accurate. In the reciprocal approach, the asymptotic analysis is omitted by assuming at the onset that the field incident on the sample and radiated by the imaginary source at the position of the detector is a plane wave. The asymptotic analysis that is required to estimate the error made by adopting this assumption is identical

to that used in the direct problem. The second reason for considering the direct problem from the start is that this way it is easier to find physical explanations for observed fluorescence phenomena, because one is not tempted to think reciprocally. A sound understanding of the physics is required to be able to achieve our ultimate goal, which is the reconstruction of the sample (elemental compositions, layer thicknesses, and layer densities) from measured fluorescence data.

In Sec. IV, we will consider primary fluorescence, which results from the direct excitation of atoms by the radiation of the x-ray tube, as well as secondary and higher-order fluorescence, which is induced by the fluorescence of other atoms. We will show that secondary fluorescence can contribute more than 25% to the measured signal and that this contribution is not constant as a function of the emission angle. Therefore, secondary (and also higher-order) effects will be taken into account in the model.

In Sec. V, we will verify the validity of the derived expressions by comparison with experiments. In the first experiment, the $K\alpha$ fluorescence from a Si layer on a Au substrate is measured. The fringes in the fluorescence intensity as a function of the emission angle will be explained using the derived formulas. In the second experiment, the secondary fluorescence from Co, due to fluorescence from a thick underlying Cu substrate, will be demonstrated. The third experiment concerns the analysis of submonolayer amounts. For the case of Co on a Si substrate, measured and computed fluorescence intensities will be compared.

II. SOURCE IN A MULTILAYER

We will consider a radiating point source inside a stratified medium consisting of M homogeneous layers. The radiated power of the source will be calculated in Sec. III and is assumed to be known here. Let (x,y,z) be a Cartesian coordinate system of which the z axis is perpendicular to the interfaces and for which the jth layer, with $j=1,\ldots,M-1$, is given by $z_j<z<z_{j-1}$, see Fig. 1. The Mth layer is assumed to fill the half space $z<z_{M-1}$. The half space $z>z_0$ is in a vacuum and will be referred to by index 0. It will be assumed that the electromagnetic fields depend on time through the implicit factor $\exp(-i\omega t)$, with $\omega=2\pi c/\lambda$, where c is the speed of light in a vacuum and λ is the wavelength in a vacuum of the radiation emitted by the source. Let $n_j=n_j'+in_j''$ be the complex refractive index of layer j corresponding to the wavelength λ. The assumed time dependence implies that the imaginary parts n_j'' are nonnegative numbers. It is customary to write

$$n_j'=1-\delta_j,\quad n_j''=\beta_j. \tag{2.1}$$

We have $\delta_0=\beta_0=0$, while for $j\neq 0$, δ_j and β_j are very small numbers, typically of the order of 10^{-3} or less. Usually and, in particular, in the examples discussed in this paper, the δ_j are positive. Hence the real parts of the refractive indices of the layers of the sample are smaller than 1.

Because the relative difference between the transmission coefficients for TE and TM polarized plane waves incident at a surface of discontinuity is of the order of the relative difference between the refractive indices of the adjacent media, the scalar theory may be used. Let the source be in point $\mathbf{r}_s=(x_s,y_s,z_s)$ of layer j_s and let P be the radiated power. If u is a component of the electric field, then the following holds:

$$k^2n_j^2u+\triangle u=0 \quad \text{inside layer } j,\ \text{with } j\neq j_s, \tag{2.2}$$

$$k^2n_{j_s}^2u+\triangle u=-(4\pi P)^{1/2}\delta(\mathbf{r}-\mathbf{r}_s) \quad \text{inside layer } j_s. \tag{2.3}$$

The source strength in the right-hand side is chosen so that $|u|^2$ is the intensity of the radiation. At the interfaces, we impose the conditions that are valid for the electrical field in the case of TE polarized fields, i.e., we demand that u and $\partial u/\partial z$ are continuous. Furthermore, for $z\rightarrow\pm\infty$, the field has to satisfy Sommerfeld's radiation conditions, which state that the field is a superposition of plane waves propagating away from the sample.

By Fourier transforming u with respect to x and y, the partial differential equations (2.2), (2.3) can be reduced to ordinary differential equations for every Fourier component. By inverse Fourier transforming the general solutions of these equations, one obtains the plane-wave expansion of the field inside all layers. In layer j with $j\neq j_s$, the plane-wave expansion is written as

$$\begin{aligned}u(x,y,z)=\int\int\{&A_j(k_x,k_y)\exp(-ik_{z,j}z)\\&+B_j(k_x,k_y)\exp(ik_{z,j}z)\}\\&\times\exp(ik_xx+ik_yy)\,dk_x\,dk_y,\end{aligned} \tag{2.4}$$

where

$$k_{z,j}=(k^2n_j^2-k_x^2-k_y^2)^{1/2}, \tag{2.5}$$

and $k=2\pi/\lambda$, with λ being the wavelength in a vacuum. We will use the branch of the square root for which the cut is along the negative x axis, $z^{1/2}$ is positive real when z is positive real, and $z^{1/2}$ is positive imaginary when z is negative real. Then $k_{z,j}$ is always in the first quadrant of the complex plane. Inside layer j_s, which contains the point source, the plane-wave expansion can be written as

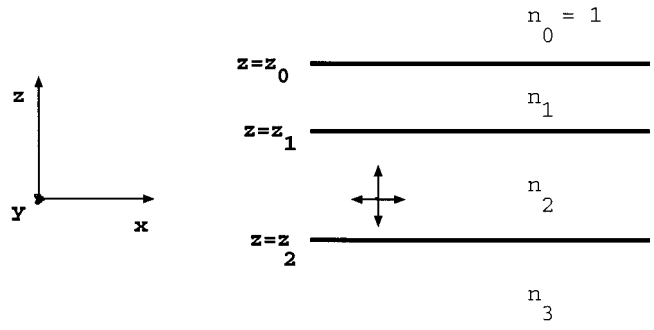

FIG. 1. Source in a multilayer sample.

$$u(x,y,z)=\int\int\{A_{j_s}(k_x,k_y)\exp(-ik_{z,j_s}z)+B_{j_s}(k_x,k_y)\exp(ik_{z,j_s}z)\}\exp(ik_xx+ik_yy)dk_xdk_y$$

$$-\frac{1}{\pi}\left(\frac{P}{4\pi}\right)^{1/2}H(z-z_s)\int\int\frac{\sin[k_{z,j_s}(z-z_s)]}{k_{z,j_s}}\exp[ik_x(x-x_s)+ik_y(y-y_s)]dk_xdk_y, \tag{2.6}$$

where H is Heaviside's function: $H(z)=1$ if $z>0$ and $H(z)=0$ if $z<0$. The integral in (2.4) and the first integral of (2.6) are solutions of the homogeneous equations, while the second integral in (2.6) is a particular solution of the equation in layer j_s with the source term on the right-hand side.

The Sommerfeld radiation conditions imply that $A_0(k_x,k_y)=B_M(k_x,k_y)=0$ for all k_x,k_y. When there are many layers, the solutions for the remaining amplitudes $A_j(k_x,k_y)$ and $B_j(k_x,k_y)$ cannot be written in closed form. However, for every k_x,k_y they can be determined by implementing a recursion formula derived from the demand that the field u and its derivative $\partial u/\partial z$ are continuous across the interfaces $z=z_j$ for $j=0,\ldots,M-1$.[17]

The calculation of the field, due to one point source based on (2.4) and (2.6), requires the numerical evaluation of two-dimensional Fourier integrals. The main interest is the total fluorescence intensity of a particular layer at the detector and since its computation requires the integration of the contributions of individual point sources it would, in general, be too time consuming to employ (2.4) and (2.6) as they stand. However, we will make use of the fact that the wavelength λ and the layer thicknesses are small compared with the distance in the z direction of the detector to the sample to expand the integrals in (2.4) and (2.6) asymptotically.

III. EXPRESSION FOR THE FIELD IN $Z>Z_0$

We consider the field in a point $\mathbf{r}=(x,y,z)$ inside the vacuum region ($z>z_0$), due to a point source in (x_s,y_s,z_s) inside the sample ($z_s<z_0$). Since $A_0(k_x,k_y)=0$ for all k_x and k_y, we have by (2.4),

$$u(x,y,z)=\int\int B_0(k_x,k_y)\exp(ik_xx+ik_yy+ik_{z,0}z)dk_xdk_y. \tag{3.1}$$

The amplitudes $B_0(k_x,k_y)$ depend on the position of the source.

The following asymptotic result will be applied. The mapping

$$(\xi,\eta)\rightarrow\xi(x-x_s)+\eta(y-y_s)+(1-\xi^2-\eta^2)^{1/2}(z-z_s), \tag{3.2}$$

has a unique stationary point (ξ_0,η_0), which is given by

$$\xi_0=\frac{(x-x_s)}{|\mathbf{r}-\mathbf{r}_s|},\quad \eta_0=\frac{(y-y_s)}{|\mathbf{r}-\mathbf{r}_s|}. \tag{3.3}$$

Let f be an arbitrary radial function. Then, by a straightforward application of the method of stationary phase,[18] one finds that for $k\rightarrow\infty$,

$$\frac{ik}{8\pi^2}\int\int\frac{f(\sqrt{\xi^2+\eta^2})}{(1-\xi^2-\eta^2)^{1/2}}\exp\{ik[\xi(x-x_s)+\eta(y-y_s)$$

$$+(1-\xi^2-\eta^2)^{1/2}(z-z_s)]\}d\xi\,d\eta$$

$$\sim\frac{1}{4\pi}f(\cos\theta)\frac{\exp(ik|\mathbf{r}-\mathbf{r}_s|)}{|\mathbf{r}-\mathbf{r}_s|}, \tag{3.4}$$

where θ is the angle between $\mathbf{r}-\mathbf{r}_s$ and the plane $z=z_0$:

$$\cos\theta=\frac{[(x-x_s)^2+(y-y_s)^2]^{1/2}}{|\mathbf{r}-\mathbf{r}_s|}. \tag{3.5}$$

The error made in the approximation is of the order

$$\frac{1}{k^{1/2}|\mathbf{r}-\mathbf{r}_s|^{1/2}\sin\theta}. \tag{3.6}$$

We shall apply result (3.4) to the integral over plane waves in expression (3.1) for the field in a point $\mathbf{r}$ in the vacuum region $z>z_0$, due to a radiating source in either the upper or lower layer of a two-layer sample. After substituting $\xi=k_x/k$ and $\eta=k_y/k$ and by using $k_{z,0}=k(1-\xi^2-\eta^2)^{1/2}$, the integral in (3.1) will be transformed to a form similar to (3.4). The deriviation for the two-layer sample given below can be readily generalized to a source inside a multilayer with an arbitrary number of layers.

If $\mathbf{r}$ is the position vector of the detector and $\mathbf{r}_s$ is the position vector of a source inside the sample, then $|\mathbf{r}-\mathbf{r}_s|$ is of the order of 10 cm. Hence, only for very small angles θ, which, in practice, are below the critical angle, may the relative error (3.6) made in using approximation (3.4) not be small.

A. Source in upper layer of two-layer sample

The reflection and transmission coefficients for a plane wave with a wave vector $(k_x,k_y,k_{z,j+1})$ inside layer $j+1$ and incident at interface $z=z_j$ are given by

$$r_j^+=\frac{k_{z,j+1}-k_{z,j}}{k_{z,j+1}+k_{z,j}},\quad t_j^+=\frac{2k_{z,j+1}}{k_{z,j+1}+k_{z,j}}. \tag{3.7}$$

For a plane wave impinging at interface $z=z_j$ from the side of layer j the reflection and transmission coefficients are

$$r_j^-=-r_j^+,\quad t_j^-=\frac{k_{z,j}}{k_{z,j+1}}t_j^+. \tag{3.8}$$

For a sample with only two layers, the amplitudes $A_j(k_x,k_y)$, $B_j(k_x,k_y)$ of the plane-wave expansions can be determined explicitly. When the point source with position

vector $\mathbf{r}_s=(x_s,y_s,z_s)$ is inside the uppermost layer $(z_1<z_s<z_0)$, one finds for the amplitude of the plane wave in the vacuum region,

$$B_0(k_x,k_y)=\frac{t_0^+}{k_{z,1}}\exp[ik_{z,1}(z_0-z_s)-i(k_xx_s+k_yy_s+k_{z,0}z_0)]\times\frac{i}{2\pi}\left(\frac{P}{4\pi}\right)^{1/2}(\chi_e+\chi_0), \tag{3.9}$$

with

$$\chi_e=\frac{1}{1-r_0^+r_1^-\exp[2ik_{z,1}(z_0-z_1)]}, \tag{3.10}$$

$$\chi_0=\frac{r_1^-\exp[2ik_{z,1}(z_s-z_1)]}{1-r_0^+r_1^-\exp[2ik_{z,1}(z_0-z_1)]}. \tag{3.11}$$

By expanding the denominator in (3.10) and (3.11), one sees that χ_e is the contribution to the amplitude B_0 of the direct ray and of rays having suffered an even number of reflections. χ_0 is the contribution of rays that have reflected an odd number of times.

The integral (3.1) can be written in the form (3.4) by changing to integration variables $\xi=k_x/k$ and $\eta=k_y/k$ and by defining

$$f(\sqrt{\xi^2+\eta^2})=t_0^+\frac{k_{z,0}}{k_{z,1}}\exp[i(k_{z,1}-k_{z,0})(z_0-z_s)]\times(4\pi P)^{1/2}(\chi_e+\chi_0). \tag{3.12}$$

Note that after the introduction of ξ and η, the common factor k can be eliminated from the reflection and transmission coefficients and that these then become functions of $\xi^2+\eta^2$ only. But f still depends on k through the exponential functions in (3.12) and we can, therefore, not apply the asymptotic result (3.4) without further justification. After writing f as a sum of terms, each containing only one exponential function, we could, in principle, apply the method of stationary phase to each of these terms individually. But the stationary points of the corresponding exponents cannot be determined explicitly and have to be computed numerically. These stationary points are very close to the stationary point (3.3) of mapping (3.2). The stationary points are so close, because the exponents occurring in f contain distances measured along the z axis, between points inside the multilayer, whereas the mapping (3.2) contains $z-z_s$, which is much larger when z corresponds to the detector. It is, therefore, sufficiently accurate to use stationary point (3.3). This means that we can use (3.4), with f given by (3.12), as if this f were not dependent on k. We, thus, obtain

$$u(\mathbf{r})\sim t_0^+\frac{k_{z,0}}{k_{z,1}}\exp[i(k_{z,1}-k_{z,0})(z_0-z_s)]\times\left(\frac{P}{4\pi}\right)^{1/2}\frac{\exp(ik|\mathbf{r}-\mathbf{r}_s|)}{|\mathbf{r}-\mathbf{r}_s|}(\chi_e+\chi_0), \tag{3.13}$$

where in $k_{z,1}$, $k_{z,0}$ and in r_0^+, r_1^- and t_0^+ the quantity $(k_x^2+k_y^2)^{1/2}$ must be replaced by $k\cos\theta$. Hence, we have in (3.13):

$$k_{z,0}=k\sin\theta,\quad k_{z,1}=k(n_1^2-\cos\theta)^{1/2}, \tag{3.14}$$

$$t_0^+=\frac{2(n_1^2-\cos^2\theta)^{1/2}}{(n_1^2-\cos^2\theta)^{1/2}+\sin\theta}, \tag{3.15}$$

$$r_0^+=\frac{(n_1^2-\cos^2\theta)^{1/2}-\sin\theta}{(n_1^2-\cos^2\theta)^{1/2}+\sin\theta}, \tag{3.16}$$

$$r_1^-=\frac{(n_1^2-\cos^2\theta)^{1/2}-(n_2^2-\cos^2\theta)^{1/2}}{(n_1^2-\cos^2\theta)^{1/2}+(n_2^2-\cos^2\theta)^{1/2}}. \tag{3.17}$$

We remark that the first factor $t_0^+k_{z,0}/k_{z,1}$ at the right of (3.13) equals t_0^-. This transmission factor appears of course also in the expression of the field that is the solution of the reciprocal problem in which the source is at $\mathbf{r}_s$ and the detector is at $\mathbf{r}$. As a matter of fact, the occurrence of transmission coefficient t_0^- in the asymptotic solution (3.13) of the direct problem is an illustration of the reciprocity theorem.

At a point in the vacuum region with position vector $\mathbf{r}$, the flux of energy in the direction of $\mathbf{r}-\mathbf{r}_s$ is in a good approximation given by $I_s(\mathbf{r})=|u(\mathbf{r})|^2$. Let the origin of the coordinate system be somewhere inside the sample. Then we have

$$I_s(\mathbf{r})=|t_0^-|^2\exp[-2\,\mathrm{Im}k_{z,1}(z_0-z_s)]\frac{P}{4\pi r^2}\times\left|\frac{1}{1-r_0^+r_1^-\exp[2ik_{z,1}(z_0-z_1)]}+\frac{r_1^-\exp[2ik_{z,1}(z_s-z_1)]}{1-r_0^+r_1^-\exp[2ik_{z,1}(z_0-z_1)]}\right|^2. \tag{3.18}$$

Some additional approximations have been made in the derivation of this result. In the denominator of the third factor, $|\mathbf{r}-\mathbf{r}_s|$ has been replaced by r. This is legitimate when $\mathbf{r}$ corresponds to the position of the detector. Furthermore, for the angle θ occurring in (3.14), (3.15), (3.16), and (3.17), it is sufficiently acccurate to use the definition

$$\cos\theta=\frac{(x^2+y^2)^{1/2}}{r}, \tag{3.19}$$

instead of (3.5). The unit for I_s is the number of photons per sec (cps) that passes a unit of surface perpendicular to $\mathbf{r}$. It is seen that I_s depends on the distance r between the detector and the sample, on the angle θ, which the detector makes with the sample surface and on the depth z_s of the source. Furthermore, in the approximations used, it depends on the source position only through z_s. By multiplying I_s by $4\pi r^2$, we get the number of photons emitted per sec in the direction of θ per unit of solid angle. This quantity is also referred to as the intensity but, contrary to I_s, it depends only on θ and not on r. In order to prevent confusion, we shall denote it by $\mathscr{I}_s$:

$$\mathscr{I}_s(\theta;z_s)=4\pi r^2I_s(\mathbf{r}). \tag{3.20}$$

It is easy to interpret expression (3.18). The third factor on the right-hand side of (3.18), $P/(4\pi r^2)$, is the intensity of the point source in a vacuum. The second (exponential) fac-

tor takes losses into account when the ray propagates from the source to the upper surface $z=z_0$. Because $n_1'<1$, there is a critical angle θ^{crit}, such that

$$\cos\theta^{\text{crit}}=n_1'. \tag{3.21}$$

For angles θ smaller than the critical angle, the imaginary part of $k_{z,1}=k(n_1^2-\cos^2\theta)^{1/2}$ becomes large. The rays detected under these angles are evanescent in the z direction inside the uppermost layer and hence, except for sources very close to the surface $z=z_0$, the detected intensity is low. The first factor on the right of (3.18), $|t_0^-|^2$, represents the change in the field strength upon transmission through the upper surface. If reflections at the interface $z=z_1$ may be neglected, i.e., when $r_1^+\approx 0$, the detected intensity due to the point source is in good approximation given by the product of the aforementioned three factors. However, for small values of θ, reflections may, in general, not be neglected. The first of the two ratios of the last factor is the contribution from the direct rays and from rays that are reflected an even number of times at the interfaces $z=z_0$, $z=z_1$. The second ratio in the fourth factor is the contribution from rays that have undergone an odd number of reflections (see Fig. 2).

Let the function $P(\mathbf{r}_s)$ be the fluorescence power per unit of sample volume corresponding to a particular fluorescence line of an element in the upper layer. The total fluorescence intensity of that line, due to the atoms in the upper layer, expressed in units of number of photons of the line per second and per unit of solid angle, is obtained by integrating (3.20) with $P=P(\mathbf{r}_s)$ over $\mathbf{r}_s$ inside the region irradiated by the tube. In the GEXRF setup, the x-ray tube irradiates a circular part of the surface of the sample almost uniformly. The fluorescence power density is, therefore, only a function of depth z_s and if we define the function $p(z_s)=\pi R_{\text{tube}}^2 P(z_s)$, where R_{tube} is the radius of the irradiated region, then $p(z_s)$ is the number of photons emitted per sec and per unit of length in the z direction by the atoms in the plane $z=z_s$. The total fluorescence intensity in unit of cps per steradian, from the upper layer observed at an angle θ with the sample surface is then

$$\mathcal{I}(\theta)=\int_{z_1}^{z_0}|t_0^-|^2\exp[-2\ \mathrm{Im}k_{z,1}(z_0-z_s)]p(z_s)\times\left|\frac{1}{1-r_0^+r_1^-\exp[2ik_{z,1}(z_0-z_1)]}+\frac{r_1^-\exp[2ik_{z,1}(z_s-z_1)]}{1-r_0^+r_1^-\exp[2ik_{z,1}(z_0-z_1)]}\right|^2 dz_s. \tag{3.22}$$

B. Source in lower layer of two-layer sample

When the source is inside the lower layer: $z_s<z_1$, the amplitude B_0 is given by

$$B_0(k_x,k_y)=\frac{t_0^+t_1^+}{k_{z,2}}\exp[ik_{z,2}(z_1-z_s)+ik_{z,1}(z_0-z_1)-i(k_xx_s+k_yy_s+k_{z,0}z_0)]\times\frac{i}{2\pi}\left(\frac{P}{4\pi}\right)^{1/2}\frac{1}{1-r_0^+r_1^-\exp[2ik_{z,1}(z_0-z_1)]}. \tag{3.23}$$

By a deriviation similar to that of (3.13) in Sec. IIIA, we find that the field at a point $\mathbf{r}$ inside the vacuum region is given by

$$u(\mathbf{r})=t_0^+t_1^+\frac{k_{z,0}}{k_{z,2}}\exp[ik_{z,2}(z_2-z_s)+ik_{z,1}(z_0-z_1)-ik_{z,0}(z_0-z_s)]\left(\frac{P}{4\pi}\right)^{1/2}\frac{\exp(ik|\mathbf{r}-\mathbf{r}_s|)}{|\mathbf{r}-\mathbf{r}_s|}\times\frac{1}{1-r_0^+r_1^-\exp[2ik_{z,1}(z_0-z_1)]}. \tag{3.24}$$

The intensity (in cps per steradian) in the direction of θ defined by (3.19), is then

$$\mathcal{I}_s(\theta;z_s)=|t_0^-t_1^-|^2\exp[-2\ \mathrm{Im}k_{z,2}(z_1-z_s)-2\ \mathrm{Im}k_{z,1}(z_0-z_1)]P\times\left|\frac{1}{1-r_0^+r_1^-\exp[2ik_{z,1}(z_0-z_1)]}\right|^2, \tag{3.25}$$

where we used $t_0^+t_1^+k_{z,0}/k_{z,2}=t_0^-t_1^-$ and where the same approximations have been made as in the derivation of (3.18). Formula (3.25) depends on the position of the source only through z_s. Again, the interpretation of the result is straightforward. The third factor, P, is the intensity (expressed in number of photons per sec and per steradian) of the point source in the vacuum. The exponent in the second factor incorporates the losses of the rays along the path from the source to the upper surface $z=z_0$. We have two critical angles, θ_0^{crit} and θ_1^{crit}, corresponding to interfaces $z=z_0$ and $z=z_1$, respectively. They are defined by

$$\cos\theta_0^{\text{crit}}=n_1', \quad \cos\theta_1^{\text{crit}}=n_2'. \tag{3.26}$$

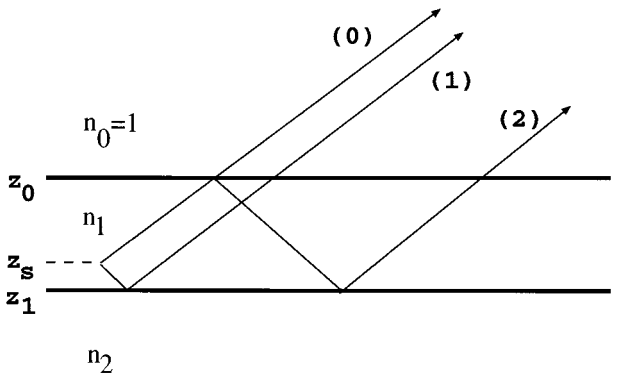

FIG. 2. Reflections of rays emitted by a source in the upper layer of a two-layer sample.

For values of θ smaller than $\theta_1^{\rm crit}$, $\mathrm{Im}k_{z,2} = k\ \mathrm{Im}(n_2^2-\cos^2\theta)^{1/2}$ is large and the wave is evanescent in the z direction inside layer 2. Hence, except perhaps for sources very close to the interface $z=z_1$, the intensity is very small. For angles smaller than the critical angle $\theta_0^{\rm crit}$, Im $k_{z,1}$ is very large and consequently the waves are evanescent in the z direction in the uppermost layer. Except when this layer is very thin, the intensity is very small at these angles. The first factor, $|t_0^- t_1^-|^2$, accounts for the change in field strength upon transmission through the interfaces $z=z_1$ and $z=z_0$. Finally, when the last factor of (3.25) is expanded, it becomes clear that it incorporates interferences, due to multiple reflections (Fig. 3).

As for the upper layer, let $P(z_s)$ be the fluorescence power per unit of sample volume for a particular line and element inside the lower layer. This density again depends only on the depth coordinate. If we again define $p(z_s)=\pi R_{\rm tube}^2 P(z_s)$, the total intensity in the direction of θ (expressed in the number of photons per second and per steradian), due to all the atoms in layer 2, becomes

$$\mathscr{I}(\theta)=\int_{-\infty}^{z_1}|t_0^- t_1^-|^2\exp[-2\ \mathrm{Im}k_{z,2}(z_1-z_s) - 2\ \mathrm{Im}k_{z,1}(z_0-z_1)]p(z_s) \times\left|\frac{1}{1-r_0^+ r_1^- \exp[2ik_{z,1}(z_0-z_1)]}\right|^2 dz_s . \quad (3.27)$$

IV. FLUORESCENCE POWER

The fluorescence intensity of a particular line and element in one of the layers of a two-layer sample at points above the sample is given by (3.22) and (3.27). The calculation of this intensity requires the determination of the fluorescence power function $p(z_s)$, i.e., of the number of photons emitted per second and per unit of depth by the atoms situated in the plane $z=z_s$. In this section, $p(z_s)$ will be computed.

The major contribution to the fluorescence power is the so-called primary fluorescence, which results from excitation directly by the radiation of the tube. Secondary fluorescence can contribute to the total fluorescence of a particular line with a wavelength λ when there is fluorescence at another line with a higher energy than that corresponding to the absorption edge of the line with the wavelength λ. Tertiary and higher-order fluorescence are analogously defined.

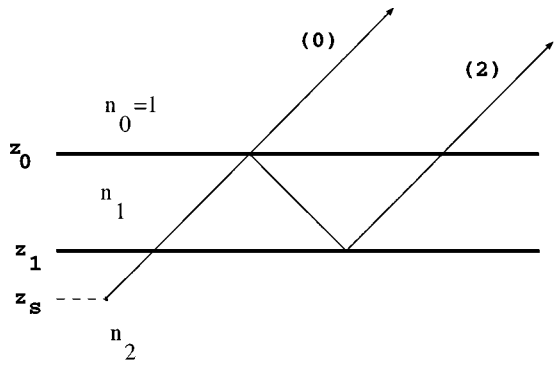

FIG. 3. Reflections of rays emitted by a source in the lower layer of a two-layer sample.

We will first compute the primary fluorescence and will then consider secondary and higher-order fluorescence. For generality the sample will be allowed to consist of an arbitrary number of layers. The mass scattering will be neglected in the calculation.

A. Primary fluorescence

We will largely adhere to the notation used in Ref. 19. The tube emits a continuous spectrum on which a few characteristic lines of the target elements are superimposed. The tube spectrum is modeled quantitatively using the algorithm proposed by Pella, Feng, and Small.[20] Let $I(\lambda_t)d\lambda_t$ be the number of photons impinging on the sample surface per second, having wavelengths in the interval $(\lambda_t,\lambda_t+d\lambda_t)$. Let ψ be the angle between the incident radiation and the normal to the sample surface. If $\mu_j(\lambda_t)$ is the mass absorption coefficient of layer j at wavelength λ_t and ρ_j is the density of the layer, then the imaginary part of the refractive index of this layer at wavelength λ_t is given by $n_j''(\lambda_t) = (\lambda_t/4\pi)\mu_j(\lambda_t)\rho_j$. Due to absorption, the intensity of the radiation at wavelength λ_t at position z inside layer j is then

$$I(\lambda_t,z)d\lambda_t = I(\lambda_t)d\lambda_t \exp\left\{-\frac{1}{\cos\psi}\left[\sum_{l=1}^{j-1}\mu_l(\lambda_t)\rho_l(z_{l-1}-z_l) + \mu_j(\lambda_t)\rho_j(z_{j-1}-z)\right]\right\}. \quad (4.1)$$

The absorbed power of radiation of wavelength λ_t per unit of depth z and per unit of wavelength is given by

$$W(\lambda_t,z)=\frac{\partial}{\partial z}I(\lambda_t,z) = \frac{\mu_j(\lambda_t)\rho_j}{\cos\psi}I(\lambda_t,z). \quad (4.2)$$

If $\mu^i(\lambda_t)$ is the mass absorption coefficient of element i and C_j^i is the relative concentration of element i in layer j, then one has

$$\mu_j(\lambda_t)=\sum_i \mu^i(\lambda_t)C_j^i . \quad (4.3)$$

The fraction of the absorbed power that can be attributed to element i is thus $\mu^i(\lambda_t)C_j^i/\mu_j(\lambda_t)$. The fluorescence power of a particular line, with a wavelength λ of element i inside layer j, is proportional to this fraction. The factor of proportionality is called the excitation factor $\mathscr{E}(\lambda,\lambda_t)$. It is the product of three probabilities: the probability of the excitation of the atom to the required level, the probability of the emission of a photon from the required level, and the probability of the emission of a photon of wavelength λ. The excitation factor depends on the fluorescence wavelength λ and on the absorbed wavelength λ_t. In order to obtain the total primary fluorescence power of the line with the wavelength λ, we have to integrate over the part of the spectrum of the x-ray tube that has a higher energy than that corresponding to the absorption edge of the line. Hence

$$p_{\text{prim}}(z)=\int_{\lambda_t<\lambda_e(\lambda)}\mathscr{E}(\lambda,\lambda_t)\mu^i(\lambda_t)I(\lambda_t,z)d\lambda_t\frac{\rho_j C_j^i}{\cos\psi}, \quad (4.4)$$

where $\lambda_e(\lambda)$ is the wavelength corresponding to the absorption edge for the line with a wavelength λ. At the values of λ_t corresponding to the characteristic lines in the tube spectrum, $I(\lambda_t)$ is a δ function. Hence, the contribution of these lines is also contained in the integral (4.4). It follows from the definition of the unit for $I(\lambda_t)$ that $p_{\text{prim}}(z)$ is expressed in the number of photons emitted per second and per unit of length in the z direction. The numerical data for physical parameters used in the equations in this section are taken from the compilations by Henke, Gullikson, and Davis[21] and de Boer.[22]

B. Secondary fluorescence

Suppose that there is fluorescence at wavelengths λ and λ', with $\lambda'<\lambda_e(\lambda)$. Then the fluorescence at wavelength λ' contributes to the fluorescence at wavelength λ. In order to be able to compute this contribution, we have to determine the field at points inside the sample due to a distribution of point sources emitting radiation of wavelength λ'. Let $P(\lambda',z_s)$ be the radiated power per unit of sample volume of the point sources. This power density is assumed to have been calculated already and depends on the depth coordinate only. The field at a point $\mathbf{r}=(x,y,z)$ corresponding to a point source at $\mathbf{r}_s$ inside layer j_s will be denoted by $u(\mathbf{r}_s,\mathbf{r})$ and is given by the Fourier integrals (2.4) and (2.6) inside the sample. The asymptotic expansion of these integrals is rather difficult. Therefore, we make the following approximations.

Because only for grazing angles the reflection and transmission coefficients of plane waves at the interfaces differ from 0 and 1, respectively, and since only a small fraction of all rays that contribute to the intensity at $\mathbf{r}=(x,y,z)$ are at grazing angles, it suffices to set all reflection and transmission coefficients in the integrals (2.4) and (2.6) equal to 0 and 1, respectively. Then, if $\mathbf{r}$ is in the same layer j_s as the point source, the asymptotic analysis yields that the field is in a good approximation given by

$$u(\mathbf{r}_s,\mathbf{r})=\left(\frac{P(\lambda',z_s)}{4\pi}\right)^{1/2}\frac{\exp\left\{\dfrac{2\pi i n_{j_s}(\lambda')}{\lambda'}|\mathbf{r}_s-\mathbf{r}|\right\}}{|\mathbf{r}_s-\mathbf{r}|}, \quad (4.5)$$

In the general case in which $\mathbf{r}$ and $\mathbf{r}_s$ can be in different layers we replace this expression by

$$u(\mathbf{r}_s,\mathbf{r})=\left(\frac{P(\lambda',z_s)}{4\pi}\right)^{1/2}\frac{\exp\left\{\dfrac{2\pi i}{\lambda'}[\mathbf{r}_s,\mathbf{r}]\right\}}{|\mathbf{r}_s-\mathbf{r}|}, \quad (4.6)$$

where $[\mathbf{r}_s,\mathbf{r}]$ is the integral of the refractive index over the line segment that links the points P_s and P of which $\mathbf{r}_s$ and $\mathbf{r}$ are the position vectors:

$$[\mathbf{r}_s,\mathbf{r}]=\int_{P_s}^{P} n\ ds. \quad (4.7)$$

Because the integration curve is straight, diffraction at the interfaces is neglected.

In a good approximation, the time-averaged Poynting vector has a length $|u(\mathbf{r}_s,\mathbf{r})|^2$ and points in the direction of $\mathbf{r}_s-\mathbf{r}$. The divergence of the negative Poynting vector is the absorbed power per unit of volume. For the source point at $\mathbf{r}_s$ that emits radiation of a wavelength λ', we find that, in a good approximation, the power absorbed per unit of volume of layer j is given by

$$W_s(\lambda',\mathbf{r})=\frac{4\pi}{\lambda'}n_j''(\lambda')|u(\mathbf{r}_s,\mathbf{r})|^2 \quad (\mathbf{r}\text{ in layer }j). \quad (4.8)$$

Because the refractive index depends on z only, one can write

$$[\mathbf{r}_s,\mathbf{r}]=[z_s,z]\frac{|\mathbf{r}_s-\mathbf{r}|}{|z_s-z|}, \quad (4.9)$$

where we use the concise notation

$$[z_s,z]\overset{\text{def.}}{=}\left[\begin{pmatrix}0\\0\\z_s\end{pmatrix},\begin{pmatrix}0\\0\\z\end{pmatrix}\right]. \quad (4.10)$$

The total absorbed power per unit of volume of layer j is obtained by integrating (4.8) over all the radiating point sources inside the cylindrical region irradiated by the tube. By using (4.10) and by switching to cylindrical integration variables centered on $\mathbf{r}$, we find for $\mathbf{r}$ in layer j:

$$\begin{aligned}W(\lambda',\mathbf{r})&=\frac{4\pi}{\lambda'}n_j''(\lambda')\int\int\int_{\substack{\text{irradiated}\\\text{region}}}\frac{P(\lambda',z_s)\exp\left\{-\dfrac{4\pi}{\lambda'}\operatorname{Im}[\mathbf{r}_s,\mathbf{r}]\right\}}{4\pi|\mathbf{r}_s-\mathbf{r}|^2}\,dx_s\,dy_s\,dz_s\\&\approx\frac{n_j''(\lambda')}{\lambda'}\int_{z_M}^{z_0}P(\lambda',z_s)dz_s\int_0^\infty\int_0^{2\pi}\frac{\exp\left\{-\dfrac{4\pi}{\lambda'}\operatorname{Im}[z_s,z][\rho^2+(z_s-z)^2]^{1/2}/|z_s-z|\right\}}{\rho^2+(z_s-z)^2}\rho\,d\rho\,d\phi\\&=\frac{2\pi}{\lambda}'n_j''(\lambda')\int_{z_M}^{z_0}P(\lambda',z_s)E_1\left(\frac{4\pi}{\lambda'}\operatorname{Im}[z_s,z]\right)dz_s,\end{aligned} \quad (4.11)$$

where E_1 is the exponential integral:

$$E_1(s)=\int_s^\infty \frac{e^{-t}}{t}\,dt. \tag{4.12}$$

In the second line, we approximated the upper integration limit for ρ by ∞. This is justified for all points $\mathbf{r}$ that are not very close to the boundary of the irradiated region. The obtained expression $W(\lambda',\mathbf{r})$ for the absorbed power can be seen to depend only on the depth z.

From here onwards, the derivation of the secondary fluorescence power density is similar to that of the primary fluorescence. By using the mass absorption coefficient (4.3), we can determine the fraction of the absorbed power of the radiation of wavelength λ' that can be attributed to the relevant element for the fluorescence at wavelength λ. Multiplication by the excitation factor $\mathscr{E}(\lambda,\lambda')$ then converts the absorbed power to fluorescence power. Because, in the irradiated region, the absorbed power (4.11) is a function of the depth coordinate only, the secondary fluorescence power $P_{\mathrm{sec}}(z)$ per unit of sample volume is also only a function of z. For convenience, we will introduce the function $p_{\mathrm{sec}}(z)=\pi R^2_{\mathrm{tube}}P_{\mathrm{sec}}(z)$, which is the secondary fluorescence power per unit of length in the z direction.

The total secondary fluorescence is obtained by summing over all the lines with wavelengths λ' satisfying $\lambda'<\lambda_e(\lambda)$. The total fluorescence power (per unit of length in the z direction) for the line with wavelength λ corresponding to element i is then the sum of the primary, secondary, and higher-order contributions. For a point of layer j, the resulting sum is

$$\begin{aligned} p(\lambda,z)=&\int_{\lambda_t<\lambda_e(\lambda)}\mathscr{E}(\lambda,\lambda_t)\mu^i(\lambda_t)I(\lambda_t,z)d\lambda_t\frac{\rho_jC_j^i}{\cos\psi}\\ &+\frac{1}{2}\sum_{\lambda'<\lambda_e(\lambda)}\mathscr{E}(\lambda,\lambda')\mu^i(\lambda')\\ &\times\int_{z_M}^{z_0}p(\lambda',z_s)E_1\left(\frac{4\pi}{\lambda'}\,\mathrm{Im}[z_s,z]\right)dz_s\;\rho_jC_j^i. \end{aligned} \tag{4.13}$$

Equation (4.13) is the recursion formula for the computation of the fluorescence power densities of all lines for which fluorescence occurs. Provided the lines are ordered in sequence of increasing absorption edge wavelength λ_e and the functions $p(\lambda,z)$ are computed in that order using (4.13), secondary, and higher-order fluorescence are all taken into account.

V. COMPARISON WITH EXPERIMENT

A. Experiment

The laboratory GEXRF spectrometer was constructed by modifying a commercial PW2400 wavelength-dispersive XRF spectrometer (Philips Analytical X-Ray, The Netherlands).[14] A module consisting of an air-cooled rotatable sample table and a double-slit collimator for direction selection was installed in the conventional spectrometer. The emission angles could be adjusted between 0 and 0.12 rad with a minimum step size of 5.0×10^{-5} rad. The angular resolution was 8.0×10^{-4} rad. Spectral selection was performed using a crystal monochromator. Sample irradiation was carried out by means of a 3 kW sealed x-ray tube having an Rh anode. Either a flow counter or a scintillation counter could be used for detection. All the experiments were carried out in a technical vacuum (of several Pa).

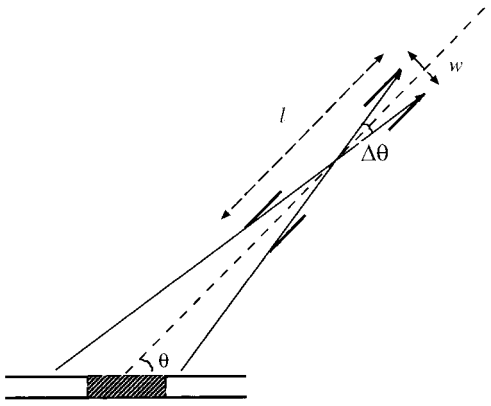

FIG. 4. The double-slit collimator. The area of the sample irradiated by the tube is shaded.

Thin-layer samples (Si/Au, Co/Si, Co/Cu) were prepared by means of electron-beam evaporation using a Balzers BAK 550 instrument (Balzers, Liechtenstein). Homogeneous layers of submonolayer coverages were prepared as follows. Silicon platelets were rendered hydrophobic through reaction with trimethyl silane dimethylamine. An aliquot of a 100 ppb Co solution was spiked with a complexing agent (ammonium pyrollidine dithiocarbamate) and was then placed on the silicon carrier. The samples were used after evaporation to dryness. The method is closely analogous to the one proposed by Knoth and Schwenke.[23]

B. Instrumental factor

To be able to compare measured and computed fluorescence intensities, we need to know the response of our instrument. We will first discuss the angular dependence of this so-called instrumental factor.

Formulas (3.22) and (3.27) are expressions for the fluorescence intensities $\mathscr{I}(\theta)$ from the upper and lower layer of a two-layer sample in the direction defined by the angle θ, with respect to the surface of the sample. They give the flux of photons per unit of solid angle. In order to be able to compute the actual number of photons measured per unit of time, $\mathscr{I}(\theta)$ has to be integrated over the solid angle suspended by the detector. This solid angle is the divergence $\Delta\theta$ of the detected beam, which satisfies $\tan(\Delta\theta/2)=w/l$, where w is the length of the shorter side of the slits and l is the distance between the slits (see Fig. 4). There is an additional weight factor $S(\theta,\theta')$ in the integration over the divergence, which depends on the geometry of the detector. When r is the effective distance between the sample and the detector, the detected power (in cps) becomes

$$P_{\mathrm{detector}}(r,\theta)=\frac{b}{4\pi r}\int_{\max\{0,\theta-(\Delta\theta/2)\}}^{\theta+(\Delta\theta/2)}S(\theta,\theta').\mathscr{I}(\theta')d\theta', \tag{5.1}$$

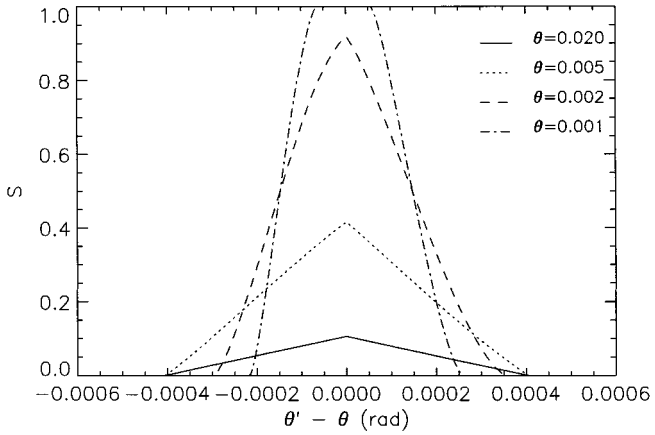

FIG. 5. The instrumental factor $S(\theta,\theta')$ for the detector used in the experiments, as a function of $\theta'-\theta$ for several values of θ. The divergence is $\Delta\theta=0.0008$ rad.

where b is the length of the longer side of the slits. For very small emission angles θ, the entire area of the sample irradiated by the tube contributes to the fluorescence, but for larger values of θ only a fraction of this area is seen by the detector. This is the main cause for the θ dependence of the instrumental factor. In Fig. 5, the instrumental factor has been plotted as a function of $\theta'-\theta$ for several values of the emission angle θ. The maximum value of S is 1; it is attained for those angles θ,θ' for which the entire area of the sample that is irradiated by the tube contributes to the detected power. For $\theta=0.005$ rad and larger values, the interval of angles θ' for which $\theta'\mapsto S(\theta,\theta')$ does not vanish is given by the divergence interval $(\theta-\Delta\theta/2,\theta+\Delta\theta/2)$ and the maximum value of S is small, because only a small fraction of the irradiated area is seen by the detector at these angles. For smaller emission angles θ, the length of the interval of contributing angles is smaller than the divergence, because the angles are limited by the irradiated area.

For a quantitive comparison of measured and calculated intensities, the efficiencies of the crystal monochromator-detector system for the various emission lines are required. These efficiencies have been calibrated by using bulk samples (very thick layers) at large emission angles.

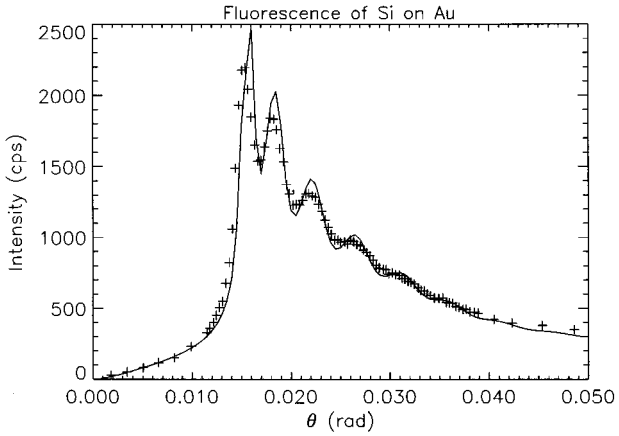

FIG. 6. Detected and computed values of Si $K\alpha$ fluorescence intensity from a 60-nm-thick Si layer on an Au substrate.

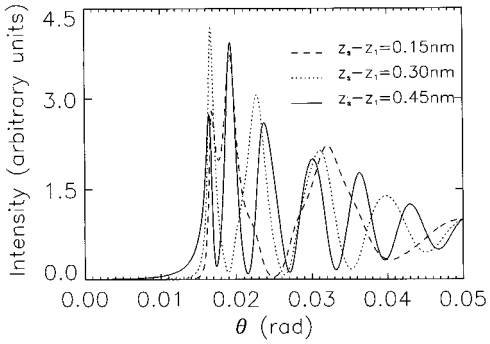

FIG. 7. Intensities I_s for three point sources inside the 60-nm-thick Si layer of Fig. 6. The point sources are at distances of one-quarter, one-half, and three-quarters of the layer thickness from the substrate. This corresponds to fringe periods of 0.024, 0.012, and 0.008, respectively.

C. Results and discussion

The detected and calculated values of the fluorescence intensity of the $K\alpha$ line ($\lambda=7.126$ Å) from a 60-nm Si layer on a thick Au substrate are shown in Fig. 6. The divergence of the double-slit collimator is sufficiently small for fringes to be visible at angles above the critical angle $\theta^{\rm crit}=0.015$ rad of the Si surface. In order to be able to understand the origin of fringes in the total intensity of the fluorescence radiation emitted by the incoherently radiating Si atoms, we will first consider the fluorescence from a single Si atom at depth z_s. This fluorescence can be computed using (3.18). The main contribution to the intensity comes from the direct beam and the beam reflected once, as shown in Fig. 2. If multiple reflections are neglected, (3.20) becomes

$$\begin{aligned}\mathcal{I}_s(\theta;z_s)=&|t_0^-|^2\exp[-2\,\mathrm{Im}k_{z,1}(z_0-z_s)]\\&\times P\{1+|r_1^-|^2\exp[-4\,\mathrm{Im}k_{z,1}(z_s-z_1)]\\&+2|r_1^-|\cos[2\,\mathrm{Re}k_{z,1}(z_s-z_1)+\mathrm{Arg}(r_1^-)]\},\end{aligned}\quad(5.2)$$

where $\mathrm{Arg}(r_1^-)$ is the change in phase suffered by the beam upon reflection at the interface $z=z_1$. The third term between the brackets corresponds to the interference between the direct beam and the beam reflected once. For angles θ not too close to the critical angle, we have

$$2\,\mathrm{Re}k_{z,1}(z_s-z_1)\approx 2\pi\frac{2(z_s-z_1)}{\lambda}\theta.\quad(5.3)$$

Hence, the period of the interference fringes in the intensity, due to one atom at depth z_s, is approximately $\lambda/[2(z_s-z_1)]$ and is thus proportional to the inverse of the distance between the atom and the interface below it. Figure 7 shows the calculated fluorescence intensities, due to three atoms at different depths. The plots are based on the "exact" formula (3.18). In contrast to Fig. 6, the instrumental factor is omitted in Fig. 7. The three sources are at distances of $d_1/4$, $d_1/2$, and $3d_1/4$, respectively, where d_1 is the thickness of the Si layer. The corresponding fringe periods $\lambda/2(z_s-z_1)$ are 0.024, 0.012, and 0.008 rad, respectively. For the Si $K\alpha$ line the refractive index of the Au substrate is considerably less than the refractive index of the Si layer.

Therefore, reflections at the interface between the Si and the Au layer are strong and this explains the large amplitudes of the fringes in Fig. 7.

Now the total fluorescence of the Si layer is obtained by integrating the intensities due to all atoms in the layer. Atoms at the same depth z_s all contribute to fringes of period (5.3). However, except when the thickness of the layer is of the order of the wavelength, integration over the depth z_s causes cancellation of the fringes. Hence, the fringes that are measured in the total fluorescence of a layer are, in general, not caused by the interference of the direct beam and the beam reflected once.

The second most important interference after that of the direct beam and the beam reflected once is that between the direct beam and the beam reflected twice. It follows from (3.18) and also immediately from Fig. 2

$$\text{fringe period}=\frac{\lambda}{2(z_0-z_1)}. \tag{5.4}$$

For the Si $K\alpha$ radiation from the 60-nm-thick layer, this yields a fringe period of 0.006 rad. Because this period is the same for all atoms, it is still visible in the integrated fluorescence intensity of the Si layer. Hence, fringes in the fluorescence intensity of the upper layer are predominantly due to the interference between the direct beam and the beam reflected twice and are, therefore, a second-order effect in the reflection coefficients. The decrease of the fringe amplitude for increasing emission angle is caused by the decrease of reflected intensities.

When fringes are visible in the detected fluorescence intensity of a particular line, the thickness of the layer can be estimated from (5.4). More accurate values for the thickness can then be obtained by fitting expression (3.22) to the intensities measured for a number of angles θ.

It is illustrative to simplify the expression for the detected power in the following way. If the divergence is small, we may replace (5.1) by

$$P_{\text{detector}}(r,\theta)\approx\frac{b}{4\pi r}\int_{\max\{0,\theta-(\Delta\theta/2)\}}^{\theta+(\Delta\theta/2)} S(\theta,\theta')d\theta'\ \mathcal{T}(\theta)$$

$$\approx\frac{b}{8\pi r}\Delta\theta S(\theta,\theta)\mathcal{T}(\theta), \tag{5.5}$$

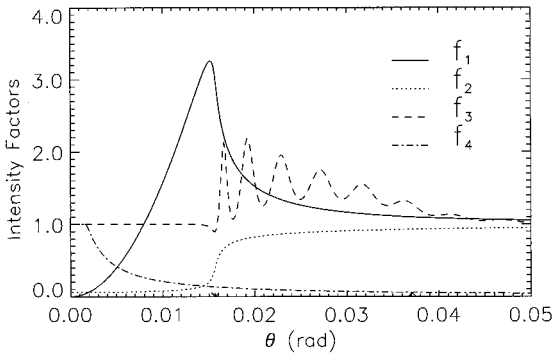

FIG. 8. The factors f_1, f_2, f_3, and f_4 defined in the text for the fluorescence intensity from the Si layer of Fig. 6.

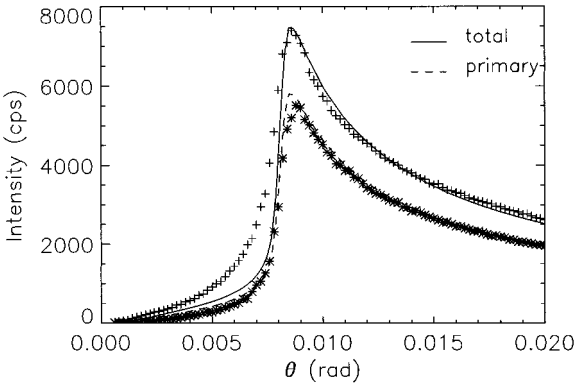

FIG. 9. Measured and computed values for the Co $K\alpha$ fluorescence intensities from a 60-nm Co layer on a thick Cu substrate (indicated by +) and on a Si substrate (indicated by *). The Cu substrate induces secondary fluorescence in Co, whereas the Si substrate does not.

where in the last line the graph of $\theta'\mapsto S(\theta,\theta')$ is approximated by a triangle (see Fig. 5). Furthermore, if the upper layer is thin, the fluorescence power density $p(z_s)$ may be considered to be constant. Then the integral over the depth that occurs in (3.22) can be computed analytically. The result is

$$\mathcal{T}(\theta)\approx|t_0^-|^2\frac{1-\exp[-2\ \mathrm{Im}k_{z,1}d_1]}{2\ \mathrm{Im}k_{z,1}d_1}pd_1$$

$$\times\frac{1+|r_1^-|^2\exp[-2\ \mathrm{Im}k_{z,1}d_1]+\psi(\theta)}{|1-r_0^+r_1^-\exp[2ik_{z,1}d_1]|^2}, \tag{5.6}$$

where $d_1=z_0-z_1$ is the thickness of the upper layer and ψ is given by

$$\psi(\theta)=4|r_1^-|\mathrm{Im}k_{z,1}d_1\frac{\exp[-2\ \mathrm{Im}k_{z,1}d_1]}{1-\exp[-2\ \mathrm{Im}k_{z,1}d_1]}$$

$$\times\frac{\sin[2\ \mathrm{Re}k_{z,1}d_1+\mathrm{Arg}(r_1^-)]-\sin[\mathrm{Arg}(r_1^-)]}{2\ \mathrm{Re}k_{z,1}d_1}. \tag{5.7}$$

In most cases $\psi(\theta)$ may be neglected. In Fig. 8, several factors occurring in (5.6) are shown for the $K\alpha$ fluorescence from the Si layer shown in Fig. 6. The first factor (f_1) to the right, $|t_0^-|^2$, incorporates the change in the field strength upon transmission through the surface $z=0$, the second factor, $f_2=[1-\exp(-2\ \mathrm{Im}k_{z,1}d_1)]/(2\ \mathrm{Im}k_{z,1}d_1)$, represents the mean, taken over all point sources, of the loss suffered by the direct ray emitted by a particular point source, propagating through the upper layer. The last factor (f_3) to the right of (5.6) and the instrumental factor in the small-divergence approximation $f_4:\theta\mapsto S(\theta,\theta)$ are also shown. Plots of these factors as functions of the angle are helpful in understanding the angular dependence of detected fluorescence intensities.

Figure 9 shows the measured and computed fluorescence intensities corresponding to the Co $K\alpha$ line of a 60-nm layer of Co on two different substrates, one consisting of Cu, the other of Si. The factors $f_1,\ldots,f_4$ of the Co fluorescence intensity on Cu are shown in Fig. 10.

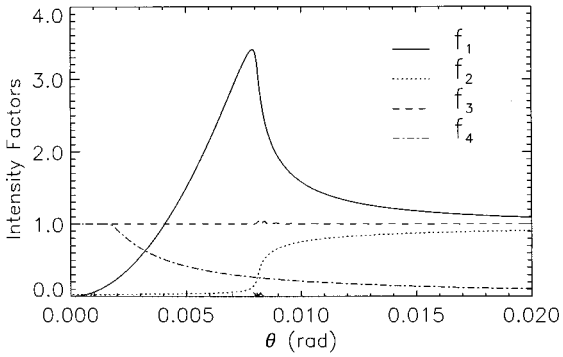

FIG. 10. The factors f_1, f_2, f_3, and f_4 of the fluorescence intensity from the Co layer on the Cu substrate in Fig. 9.

Contrary to Cu, the fluorescence of Si cannot induce the $K\alpha$ fluorescence of Co. Due to a small difference in the refractive idea of Co, Cu, and Si for the Co $K\alpha$ radiation, fringes do not occur and hence the influence of the refractive index of the substrate on the measured fluorescence of Co is small. Therefore, the measurement of the Co fluorescence on the Si substrate gives an accurate estimation of the primary fluorescence intensity in the case of the Cu substrate. This is confirmed by the results of the comparison with the computed primary fluorescence intensities shown in Fig. 9.

We used a sufficiently thick Cu substrate (5 μm), so that the secondary fluorescence amounts to $\approx$ 28% of the total Co $K\alpha$ fluorescence. Below the critical angle, the intensity of the measured fluorescence on the Cu substrate is higher than the simulated intensity. An AFM image of the sample demonstrates that roughness of the Co surface is the cause of this discrepancy. The Co surface inherits a considerable roughness from the very rough Cu substrate. For the contribution of the secondary fluorescence to be maximized, the Cu substrate has to be rather thick and this causes the Cu surface, and consequently also the Co surface, to be rough.

The computed ratio of the secondary and total fluorescence, as a function of the emission angle, is shown in Fig. 11. It can be seen that the relative contribution of the secondary fluorescence is a slowly increasing function of the detection angle with a small step at the critical angle. This increase is due to the fact that, at larger detection angles, the

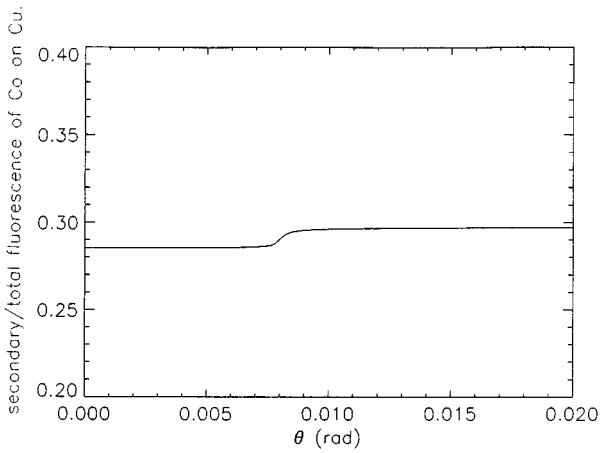

FIG. 11. Computed ratio of the secondary and total fluorescence from the Co layer on the Cu substrate in Fig. 9.

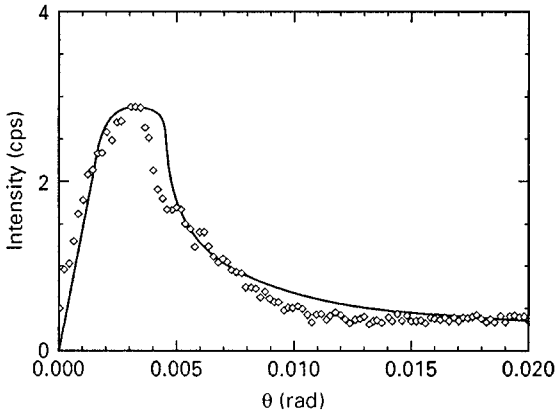

FIG. 12. Detected and computed values for the Co $K\alpha$ fluorescence of 1.4×10^{14} Co atoms/ cm^2 on Si. The best fit between the measurements and the calculations is obtained for a distance to the Si surface of 10 Å.

contribution from Co atoms that are closer to the Cu substrate and, are, therefore, more efficiently excited by the Cu, becomes more important than at smaller angles. For reasons mentioned above, the step at the critical angle could not be measured however.

The last example concerns the analysis of very dilute layers of submonolayer coverage. The detected and computed $K\alpha$ fluorescence intensities of the 1.4×10^{14} Co atoms/ cm^2 on Si are shown in Fig. 12. The shape of the curve differs from that obtained for the much thicker layers discussed above. This can be understood by considering that a layer with a thickness of one monolayer or less can be modeled as a distribution of radiating point sources all situated in the same plane in a vacuum at a certain distance from the refelecting plane. This distance has to be determined, so that the measured and computed intensities fit best.

The formula for the fluorescence of atoms that are all at the same distance z_s-z_1 to the substrate is, with the exception of the instrumental factor, given by (3.18), in which P is the total fluorescence power of the plane of fluorescent Co atoms. Because there is no interface at $z=z_0$, we have $t_0^+=1$, $r_0^+=0$, and $k_{z,1}=k_{z,0}=k\sin\theta$. Then (3.18) simplifies to

$$I(r,\theta)=\frac{P}{4\pi r^2}|1+r_1^-(\theta)\exp[2ik(z_s-z_1)\sin\theta]|^2 \tag{5.8}$$

$$\approx\frac{P}{4\pi r^2}|1+r_1^-(\theta)|^2, \tag{5.9}$$

where the dependence on θ of the reflection coefficient is emphasized and where in approximation (5.9), use has been made of the fact that the distance z_s-z_1 of the atoms to the substrate is of the order of the wavelength and the angles θ of interest are small. Hence, in a first approximation, the θ dependence of the measured fluorescence intensity is given by the θ dependence of the reflection coefficient. Below the critical angle for total reflection at the interface $z=z_1$, the absolute value of r_1^- is almost constant and equal to 1 but, as follows from (3.17), the phase of the reflection coefficient

depends on θ, so that r_1^- varies between -1 at $\theta=0$ and $+1$ at $\theta=\theta_1^{\rm crit}=n_2'$. This explains the shape of the measured intensity curve.

VI. CONCLUSION

Explicit expressions for the fluorescence intensity at grazing-emission angles from layered samples can be derived by applying asymptotics to the solution of the Helmholtz equation for a radiating point source. Avoiding the use of the optical reciprocity theorem has the benefit that the physical significance of the various terms in the general expressions for the angular dependence of the fluorescence intensity is immediately clear. Moreover, a direct understanding of the physics allows identification of the dominant terms in the equations, which leads to very simple explanations in specific cases. This can be demonstrated for the example of fringes caused by multiple reflections in a layered system and for that of a distribution of atoms of submonolayer coverage at a given distance from a reflecting surface.

ACKNOWLEDGMENTS

The authors thank Dr. H.A. van Sprang for adapting the algorithm for the computation of the spectrum emitted by the x-ray tube and Dr. D.K.G. de Boer for helpful discussions. The experimental assistance of A. G. J. Leenaers and J. C. Naismith (Strathclyde University, Glasgow) is gratefully acknowledged. The work described in this paper was performed in partial fulfillment of JESSI Project No. E106.

[1] Y. Yoneda and T. Horiuchi, Rev. Sci. Instrum. **42**, 1069 (1971).
[2] P. Wobrauschek, H. Aiginger, G. Owesny, and C. Streli, J. Trace Microprobe Techniq. **6**, 295 (1988).
[3] H. Schwenke and J. Knoth, in *Handbook of X-Ray Spectrometry*, edited by R.E. Van Grieken and A.A. Markowicz (Dekker, New York, 1993), Chap. 9.
[4] P. Eichinger, H.J. Rath, and H. Schwenke, in *ASTM STP 990*, edited by D.C. Gupta (American Society for Testing and Materials, Philadelphia, 1988), p. 305.
[5] V. Penka and W. Hub, Spectrochim. Acta Part B **44**, 483 (1989).
[6] J.M. Bloch, M. Sansone, F. Rondelez, D.G. Pfeiffer, P. Pincus, M.W. Kim, and P.M. Eisenberger, Phys. Rev. Lett. **54**, 1039 (1985).
[7] D.K.G. de Boer, Phys. Rev. B **44**, 498 (1991).
[8] G. Tölg and R. Klockenkämper, Spectrochim. Acta Part B **48**, 111 (1992).
[9] R.S. Becker, J.A. Golovchenko, and J.R. Patel, Phys. Rev. Lett. **50**, 153 (1983).
[10] S. Haegawa, S. Ino, Y. Yamamoto, and H. Daimon, Jpn. J. Appl. Phys. **24**, L387 (1985).
[11] Y.C. Sasaki and K. Hirokawa, Appl. Phys. Lett. **58**, 1384 (1991).
[12] T. Noma, A. Iida, and K. Sakurai, Phys. Rev. B **48**, 17 525 (1993).
[13] T. Noma and A. Iida, Rev. Sci. Instrum. **65**, 837 (1994).
[14] P.K. de Bokx and H.P. Urbach, Rev. Sci. Instrum. **66**, 15 (1995).
[15] L.D. Landau and E.M. Lifshitz, *Electrodynamics of Continuous Media* (Pergamon Press, Oxford, 1960), p. 288.
[16] L.G. Parratt, Phys. Rev. **95**, 359 (1954).
[17] M. Born and E. Wolf, *Principles of Optics* (Pergamon Press, Oxford, 1986).
[18] R. Wong, *Asymptotic Approximation of Integrals* (Academic Press, Boston, 1989).
[19] R. Tertian and F. Claisse, *Principles of Quantitative X-Ray Fluorescence Analysis* (Heyden & Son, London, 1982).
[20] P.A. Pella, L. Feng, and J.A. Small, X-Ray Spectrom. **14**, 125 (1985).
[21] B.L. Henke, E.M. Gullikson, and J.C. Davis, At. Data Nucl. Data Tables **54**, 181 (1993).
[22] D.K.G. de Boer, Spectrochim. Acta Part B **44**, 1171 (1989).
[23] J. Knoth and H. Schwenke, Fresenius Z. Anal. Chem. **294**, 273 (1979).